Supporting Information

Khafaga et al. 10.1073/pnas.1207866109

SI Materials and Methods

Structural Model for Na^+-K^+-ATPase–Phospholemman Complex. Molecular graphics images were produced using the chimera package from the Resource for Biocomputing, Visualization, and Informatics at the University of California at San Francisco (1). We applied the Rosetta full atom relax protocol (2–4) to homology modeling of rat Na^+-K^+-ATPase (NKA) α-subunit and human NKA β-subunit based on shark rectal gland NKA (5). We used the NMR structure of human phospholemman (PLM) (6) for homology modeling of dog PLM. We positioned the structural models of rat NKA α-subunit, human NKA β-subunit, and dog PLM based on their positions in the X-ray structure of shark rectal gland NKA (5). Ten thousand models of the NKA–PLM complex were generated followed by model clustering as described previously (7). The center of the largest cluster model was chosen as the best model.

Constructs and Site-Directed Mutagenesis. NKA and PLM were mutated using the Quickchange mutagenesis kits (QuickchangeII XL and Quickchange Lightning; Stratagene). Several CFP–NKA-α1 mutants were constructed: Ala substitutions at F956, E960, E961, L964, F967, or C145, respectively (numbering is for rat) or a truncation of the C terminus (ΔKETYY). In addition, residue F28 of PLM–YFP was mutated to both Ala and Cys. The following custom-made, forward and reverse primers were obtained from Integrated DNA Technologies (IDT): for F967A, 5′-agacagctcttgctgctgccctgtcctactgccc-3′ and 5′-gggcagtaggacagggcagcagcaagagctgtct-3′; for L964A, 5′-cctctttgaagagacagctgctgctgctttcctgtcc-3′ and 5′-ggacaggaaagcagcagcagctgtctcttcaaagagg-3′; for E960A, 5′-taatatttggcctctttgcagagacagctcttgctgc-3′ and 5′-gcagcaagagctgtctctgcaaagaggccaaatatta-3′; for F956A, 5′-ccagcagggaatgaagaacaagatcttaatagctggcctctttgaagag-3′ and 5′-ctcttcaaagaggccagctattaagatcttgttcttcattccctgctgg-3′; for E961A, 5′-atttggcctctttgaagcgacagctcttgctgctt-3′ and 5′-aagcagcaagagctgtcgcttcaaagaggccaaat-3′; for C145A, 5′-gctgtcgtcatcataactggcgctttctcctattatcaagaagc-3′ and 5′-gcttcttgataataggagaaagcgccagttatgatgacgacagc-3′; for F956A, 5′-ccagcagggaatgaagaacaagatcttaatagctggcctctttgaagag-3′ and 5′-ctcttcaaagaggccagctattaagatcttgttcttcattccctgctgg-3′; and for deletion of the C-terminal tail (ΔKETYY), 5′-cggctgggtggagtagcccactgccc-3′ and 5′-gggcagtgggctactccacccagccg-3′. For the coimmunoprecipitation experiments an HA tag was introduced to PLM. The following primers (IDT) were used consecutively: 5′-ccgtctgtccacccgcaggcggtacccatacggagctcaagcttcgaattctgc-3′ and 5′-gcagaattcgaagcttgagctccgtatgggtaccgcctgcgggtggacagacgg-3′, then 5′-acccgcaggcggtacccatacgatgttccagattacaattctgcagtcgacggtaccc-3′ and 5′-gggtaccgtcgactgcagaattgtaatctggaacatcgtatgggtaccgcctgcgggt-3′, and finally 5′-ccatacgatgttccagattacgcttaggcagtcgacggtaccccggtc-3 and 5′-gaccggggtaccgtcgactgcctaagcgtaatctggaacatcgtatgg-3′. The PCR parameters were set according to the manufacturer's instructions. After PCR, template DNA was eliminated by DpnI digestion. Mutations in the amplified DNA were confirmed by sequencing.

Culture and Transfection of HEK293 Cells. HEK293 cells (American Type Culture Collection) were cultured in DMEM with 5% (vol/vol) FBS and 5% (vol/vol) penicillin/streptomycin. To create cell lines that stably express WT or mutant rat CFP–NKA-α1, regular HEK cells were transfected with the corresponding plasmids (10 μg DNA) and cultured at low density in DMEM with 10 μM ouabain as selecting agent. Well-transfected colonies were then isolated and recultured (in the presence of 10 μM ouabain). Before experiments, cells were plated on coverslips and transiently transfected with plasmids encoding YFP-fusion construct cDNAs of wild-type and mutant PLM, respectively (5 μg DNA). Lipofectamine 2000 served as transfection reagent resulting in high transfection efficiencies with about 80% coexpression.

Average Fluorescence Resonance Energy Transfer Experiments. We coexpressed mutant CFP–NKA-α1 and WT–PLM–YFP in HEK293 cells, and measured fluorescence resonance energy transfer (FRET) using the acceptor photobleach method, as described previously (8, 9). When FRET is present, it can be prevented by photobleaching the acceptor (YFP) resulting in an increase in donor emission (CFP).

Fluorescence imaging was performed using an inverted microscope with a 1.49 NA objective, and a back-thinned CCD camera (iXon 887; Andor Technology). Both image acquisition and acceptor photobleaching were automated using MetaMorph software (Molecular Devices), with macros for controlling motorized excitation/emission filter wheels (Sutter Instrument) with filters for CFP (excitation 427/10 nm, emission 472/30 nm) and YFP (excitation 504/12 nm, emission 542/27) (Semrock). We measured CFP emission before and after photobleaching YFP. YFP was progressively photobleached using the following protocol: 100-ms acquisition of CFP image, 40-ms acquisition of YFP image, followed by repeated 10-s exposure to YFP-selective photobleaching.

Fluorescence intensity of the CFP donor before ($F_{\mathrm{Prebleach}}$) and after ($F_{\mathrm{Postbleach}}$) acceptor photobleaching was used to calculate FRET efficiency (E) according to the following relationship: $E = (F_{\mathrm{Postbleach}}/F_{\mathrm{Prebleach}}) - 1$. The FRET efficiency allows a calculation of the distance between the CFP–YFP pair using the Förster equation $R = R_0 \cdot ((1 - E)/E)^{1/6}$. R_0 is the Förster distance and amounts to 5.3 nm for the CFP–YFP pair (10).

Detailed FRET Experiments. FRET was also measured at various PLM–YFP expression levels, plotting FRET efficiency for each single region according to the corresponding relative YFP fluorescence, which was taken as an index of the relative PLM concentration of each cell. This is effectively a titration experiment with FRET efficiency fit to $\mathrm{FRET} = (\mathrm{FRET}_{\mathrm{max}})[\mathrm{YFP}]/(K_{0.5} + [\mathrm{YFP}])$, where [YFP] is the initial (unbleached) YFP concentration in the cell in arbitrary units, and FRET is the observed FRET efficiency. The equation is analogous to that in recently published work by Song et al. (11). $K_{0.5}$ is the apparent dissociation constant of the FRET complex, which provides a measure of the apparent interaction affinity. Fig. S1 shows a representative experiment with cells stably expressing CFP–E960A–NKA and transiently expressing WT–PLM–YFP. Analysis regions (regions of interest, ROI) are represented by the little circles on the cell membranes (usually one to five per cell depending on the cell size). Our criteria for placing the circles were: (*i*) stable cell membranes (i.e., no motion during imaging), (*ii*) no double membranes (i.e., avoiding apposed cell membranes because one would not be able to assign them to a particular cell), (*iii*) good contrast between membrane and cytosolic signal, and (*iv*) normal photobleaching kinetics. In addition, one region per image (see example images in Fig. S1, red circle in the *Upper Right* corner) was picked in a cell-free area (with low signal) for background subtraction.

Coimmunoprecipitation. Coimmunoprecipitation (co-IP) experiments were performed using an agarose-conjugated HA antibody (Santa Cruz Biotechnology). The immunoprecipitation (IP) conditions were as previously described (12). After cotransfecting HEK293 cells with NKA-α1 (WT or mutant) and HA-tagged PLM (WT or mutant) cells were lysed in solubilization buffer. The buffer contained 6 mg/mL n-dodecyl octaethylene glycol monoether detergent ($C_{12}E_{10}$; Calbiochem) and in millimoles: 140

NaCl, 25 imidazole, and 1 EDTA, pH 7.3. Next, detergent-free buffer was used to dilute the lysate 1:1 1 mg protein/mL and proteins were further solubilized by frequent vortexing over 30 min at 4 °C. The dilution was then centrifuged for 30 min at 20,000 × *g* and 4 °C to get rid of any debris. Cell lysates were incubated with the agarose-conjugated HA antibody overnight (4 °C; end-over-end rotation). Immunoprecipitates were obtained by centrifugation for 10 min at 10,000 × *g* and 4 °C. They were then washed five times with solubilization buffer (containing 0.05% $C_{12}E_{10}$) before the pellet was resuspended in sample buffer and centrifuged at 10,000 × *g* for 10 min. Supernatants were loaded onto gels for SDS/PAGE and proteins were transferred to 0.20-μm nitrocellulose membranes. Blocking of nonspecific binding was achieved by placing the membranes in 8% (wt/vol) milk in Tris-buffered saline before membranes were incubated overnight with primary antibody at 4 °C [GFP antibody for recombinant NKA (1:1,000 dilution; Abcam) and PLM-C2 (1:2,500 dilution)] (13). Next, membranes were incubated with secondary antibody (IRDye680RD goat antirabbit antibody from LI-COR). Blots were then captured with the Odyssey NIR fluorescent imager and analyzed using ImageJ. The NKA-to-PLM signal intensity ratio was used to quantify the amount of NKA pulled down with PLM. This ratio was normalized to the control condition (WT–NKA + WT–PLM not exposed to forskolin) so that mean data could be compiled for different experimental repeats (three different sets of IPs were done).

$[Na^+]_i$ and NKA-Mediated Na^+ Extrusion Measurements. $[Na^+]_i$ and NKA-mediated Na^+ extrusion measurements were performed as described previously (9, 14–16). HEK293 cells expressing WT or mutated NKA alone or cells coexpressing NKA with WT–PLM were loaded with sodium-binding benzofuran isophthalate acetoxymethyl ester (SBFI-AM; 10 μM) for 2 h and then exposed to normal Tyrode's solution (in millimoles: 140 NaCl, 4 KCl, 1 $MgCl_2$, 10 glucose, 5 Hepes and 1 $CaCl_2$; pH 7.4) for 20 min to allow for SBFI deesterification. Using an Optoscan monochromator (Cairn Research) fluorescence was collected at 535 ± 20 nm, while alternately exciting SBFI at 340 and 380 nm (F_{340} and F_{380}). Cells were Na^+ loaded by inhibiting NKA in a K^+-free solution containing (in millimoles): 145 NaCl, 2 EGTA, 10 Hepes, and 10 glucose (pH = 7.4). $[Na^+]_i$ decline was measured upon pump reactivation in a Na^+-free solution containing (in millimoles): 140 TEA-Cl, 4 KCl, 1 $MgCl_2$, 2 EGTA, 10 Hepes, and 10 glucose (pH = 7.4). Because cell volume does not change under this protocol (14), $[Na^+]_i$ decline reflects Na^+ efflux. One micromole of ouabain was present throughout the experiment to block endogenous NKA activity. F_{340}/F_{380} was calculated after background subtraction (at each wavelength) and converted to $[Na^+]_i$ by calibration at the end of each experiment in the presence of 10 μM gramicidin and 100 μM strophanthidin.

For analysis, the rate of $[Na^+]_i$ decline ($-d[Na^+]_i/dt$) was plotted as a function of $[Na^+]_i$ and fitted with: $-d[Na^+]_i/dt = V_{max}/(1 + (K_{0.5}/[Na^+]_i)^{nHill})$, where V_{max} is the maximum Na^+ extrusion rate, $K_{0.5}$ is the $[Na^+]_i$ for the half-maximal activation of the pump, and n_{Hill} is the Hill coefficient.

Confocal Imaging. Confocal imaging (Olympus Fluoview, laser line 440 nm) was used to check for appropriate CFP expression and correct membrane targeting of the NKA constructs (Fig. S3). The same imaging settings were used for comparing the CFP signals in the various cell lines.

Statistical Analysis. Data are expressed as means ± SEM. Statistical discriminations were performed with Student's *t* test (paired when appropriate) with $P < 0.05$ considered significant. Co-IP data were analyzed using a one-way ANOVA ($^*P < 0.01$) and Student's *t* test for pairs comparison ($^{\#}P < 0.05$).

1. Pettersen EF, et al. (2004) UCSF Chimera—a visualization system for exploratory research and analysis. *J Comput Chem* 25(13):1605–1612.
2. Yarov-Yarovoy V, Schonbrun J, Baker D (2006) Multipass membrane protein structure prediction using Rosetta. *Proteins* 62(4):1010–1025.
3. Barth P, Schonbrun J, Baker D (2007) Toward high-resolution prediction and design of transmembrane helical protein structures. *Proc Natl Acad Sci USA* 104(40):15682–15687.
4. Rohl CA, Strauss CE, Misura KM, Baker D (2004) Protein structure prediction using Rosetta. *Methods Enzymol* 383:66–93.
5. Shinoda T, Ogawa H, Cornelius F, Toyoshima C (2009) Crystal structure of the sodium-potassium pump at 2.4 A resolution. *Nature* 459(7245):446–450.
6. Teriete P, Franzin CM, Choi J, Marassi FM (2007) Structure of the Na,K-ATPase regulatory protein FXYD1 in micelles. *Biochemistry* 46(23):6774–6783.
7. Bonneau R, Strauss CE, Baker D (2001) Improving the performance of Rosetta using multiple sequence alignment information and global measures of hydrophobic core formation. *Proteins* 43(1):1–11.
8. Bossuyt J, Despa S, Martin JL, Bers DM (2006) Phospholemman phosphorylation alters its fluorescence resonance energy transfer with the Na/K-ATPase pump. *J Biol Chem* 281(43):32765–32773.
9. Bossuyt J, et al. (2009) Isoform specificity of the Na/K-ATPase association and regulation by phospholemman. *J Biol Chem* 284(39):26749–26757.
10. Elangovan M, et al. (2003) Characterization of one- and two-photon excitation fluorescence resonance energy transfer microscopy. *Methods* 29(1):58–73.
11. Song Q, Pallikkuth S, Bossuyt J, Bers DM, Robia SL (2011) Phosphomimetic mutations enhance oligomerization of phospholemman and modulate its interaction with the Na/K-ATPase. *J Biol Chem* 286(11):9120–9126.
12. Bossuyt J, Ai X, Moorman JR, Pogwizd SM, Bers DM (2005) Expression and phosphorylation of the na-pump regulatory subunit phospholemman in heart failure. *Circ Res* 97(6):558–565.
13. Silverman BZ, et al. (2005) Serine 68 phosphorylation of phospholemman: Acute isoform-specific activation of cardiac Na/K ATPase. *Cardiovasc Res* 65(1):93–103.
14. Despa S, Islam MA, Weber CR, Pogwizd SM, Bers DM (2002) Intracellular Na^+ concentration is elevated in heart failure but Na/K pump function is unchanged. *Circulation* 105(21):2543–2548.
15. Despa S, et al. (2005) Phospholemman-phosphorylation mediates the beta-adrenergic effects on Na/K pump function in cardiac myocytes. *Circ Res* 97(3):252–259.
16. Despa S, Tucker AL, Bers DM (2008) Phospholemman-mediated activation of Na/K-ATPase limits $[Na]_i$ and inotropic state during beta-adrenergic stimulation in mouse ventricular myocytes. *Circulation* 117(14):1849–1855.

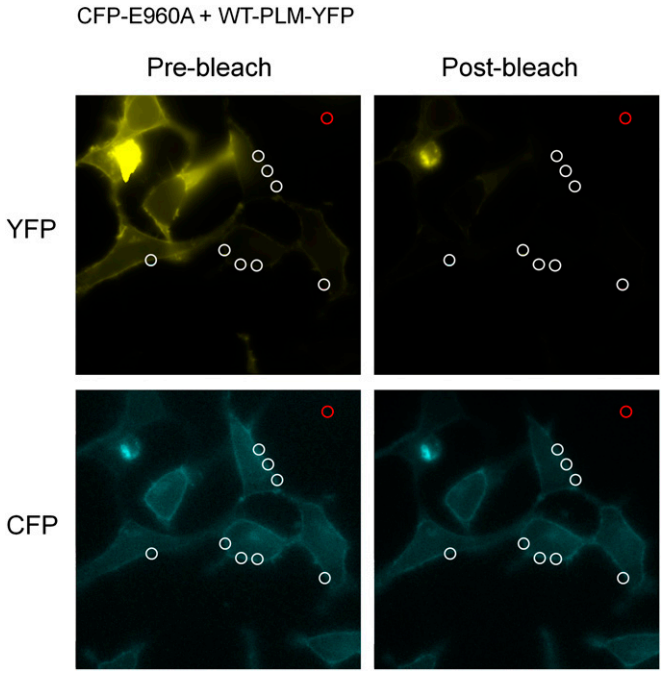

Fig. S1. Analysis regions (regions of interest, ROI) in a representative experiment with cells stably expressing CFP–E960A-NKA and transiently expressing WT–PLM–YFP. Regions are represented by the little circles on the cell membranes. The red circle in the *Upper Right* corner of each image marks the cell-free area with the lowest signal used for background subtraction.

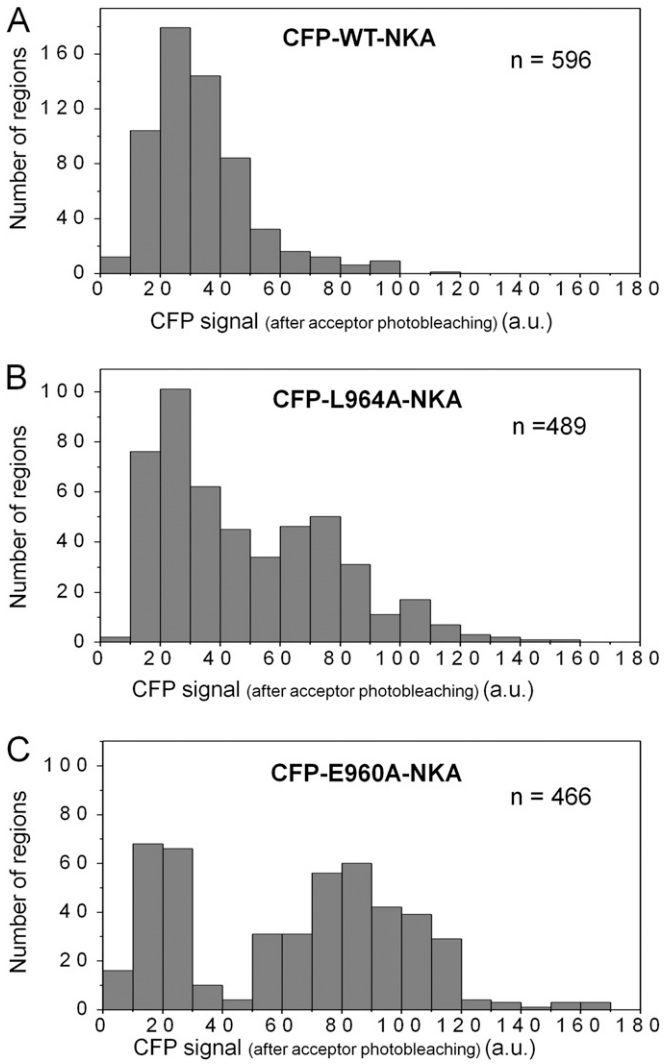

Fig. S2. CFP expression varies to a similar extent as FRET. CFP expression histograms show a wide distribution range (*A*) for WT–NKA (n = 596), (*B*) for the NKA mutant L964A (n = 489), and (*C*) for the NKA mutant E960A (n = 466).

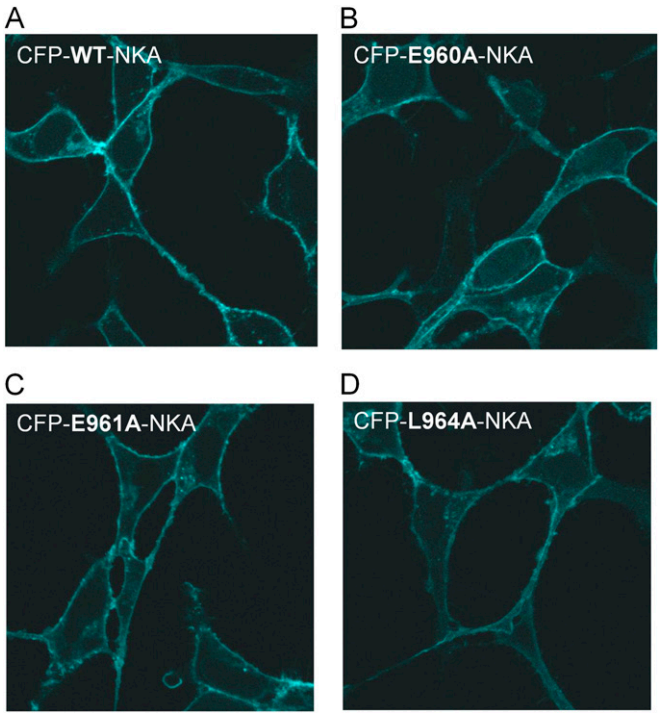

Fig. S3. Confocal images of CFP–NKA expression in the stable cell lines: CFP–WT–NKA (*A*), CFP–E960A-NKA (*B*), CFP–E961A-NKA (*C*), or CFP–L964A-NKA (*D*). All cell lines show reliable and comparable CFP expression with correct membrane targeting.